Chinese Chemical Letters 37 (2026) 112335

Contents lists available at ScienceDirect

Chinese Chemical Letters

journal homepage: www.elsevier.com/locate/cclet

Cluster airflow assisted matrix coating enhances high-resolution MALDI imaging of small molecules and lipids in tissues and cells

Hua Guo[a,1], Ran Wu[a,b,1], Qichen Hao[a,1], Liang Qin[a], Lulu Chen[a], Hao Hu[a], Jie Feng[c], Lei Wang[a], Rui Liu[a], Difan Chen[a], Anna Wang[a], Zihan Wang[a], Xiangrui Cheng[a], Shuyu Hao[d], Xiaodong Wang[a,b,*], Huaqing Zhang[e,*], Gaopeng Li[f,*]

[a] College of Life and Environmental Sciences, Centre for Imaging & Systems Biology, Minzu University of China, Beijing 100081, China
[b] College of Biological Sciences and Technology, Beijing Forestry University, Beijing 100083, China
[c] Beijing Neurosurgical Institute, Capital Medical University, Beijing 100070, China
[d] Beijing Tiantan Hospital, Capital Medical University, Beijing 100070, China
[e] Department of Clinical Engineering, School of Medicine, The Second Affiliated Hospital, Zhejiang University, Hangzhou 310009, China
[f] General Surgery Department, Shanxi Bethune Hospital, Taiyuan 030032, China

ARTICLE INFO

Article history:
Received 13 July 2025
Revised 18 November 2025
Accepted 28 December 2025
Available online 31 December 2025

Keywords:
Cluster airflow
Nano-matrix coating
Single cell
Tissue section
MALDI imaging

ABSTRACT

The matrix deposition method is one of the critical factors influencing the performance of matrix-assisted laser desorption/ionization mass spectrometry imaging (MALDI-MSI), as it determines matrix crystal sizes and coating uniformity, thereby impacting ionization efficiency and spatial resolution. Currently, automated sprayers are widely utilized for matrix deposition due to their convenience, speed, and robust reproducibility. However, existing automated spraying techniques typically produce micrometer-sized crystal particles, limiting high-resolution imaging quality and sensitivity. To overcome this, we introduce cluster airflow assisted matrix coating (CAAMC), which employs multiple cluster airflows to achieve a more uniform dispersion and atomization of the matrix droplets, resulting in nano-sized crystal particles—an advance beyond traditional deposition methods. This method represented the first successful automatic spray method for nano-matrix crystallization, surpassing regular-one channel pneumatic spraying and sublimation in producing smaller, more homogeneous crystals. Application to rat brain tissues and single cells demonstrates that CAAMC significantly enhances small molecule and lipid detection efficiency and imaging quality (lateral resolution of 5 μm), exceeding the performance of regular-one channel pneumatic spraying and sublimation. Overall, CAAMC significantly broadens the potential of automated matrix spraying techniques in high-resolution MALDI-MSI.

© 2026 Published by Elsevier B.V. on behalf of Chinese Chemical Society and Institute of Materia Medica, Chinese Academy of Medical Sciences.

Mass spectrometry imaging (MSI) is a powerful analytical technique capable of simultaneously detecting and imaging numerous compounds within biological samples, thereby providing comprehensive information regarding spatial distribution and relative abundance [1,2]. Among various MSI methodologies, matrix-assisted laser desorption/ionization MSI (MALDI-MSI) stands out as one of the most prominent techniques due to its exceptional features, including high resolution, high sensitivity, and high throughput [3]. Currently, MALDI-MSI has been extensively utilized in the investigation of the spatial distribution of small molecule metabolites [4–7], lipids [8–10], and proteins [11–13], demonstrating its unique advantages in the analysis of biological samples. Due to its outstanding performance, MALDI-MSI exhibits significant application potential in many fields, including biopharmaceuticals [14], environmental science [15,16], and pathology [17–19].

However, the detection and imaging performance of MALDI-MS is influenced by several critical factors, such as matrix type, matrix deposition method, spraying instrument, spraying conditions. Among them, the optimization of matrix deposition method is of great importance, because it determines the size of the matrix particles and the uniformity of the matrix coating [15,16]. Small matrix crystal sizes and uniform matrix coatings can effectively enhance ionization efficiency and imaging resolution, leading to high-quality imaging outcomes [4]. These imaging results can provide clearer regional distribution of compounds as well as more accurate assessments of their relative abundances. This capability facilitates the reliable differentiation of histopathological regions,

* Corresponding authors.
E-mail addresses: Xiaodong@muc.edu.cn (X. Wang), zhqnature@zju.edu.cn (H. Zhang), malone2001@163.com (G. Li).
[1] These authors contributed equally to this work.

https://doi.org/10.1016/j.cclet.2025.112335
1001-8417/© 2026 Published by Elsevier B.V. on behalf of Chinese Chemical Society and Institute of Materia Medica, Chinese Academy of Medical Sciences.

the efficient classification of cell types, and the precise identification of potential biomarkers. Additionally, smaller matrix particles can facilitate MALDI-MSI at the single-cell resolution, which is crucial for visualizing compounds within smaller biological entities such as cells, organelles, and micro-region in tissue sections. Currently, various matrix deposition methods are available, including manual spraying [20], sublimation [21,22], and automatic sprayer [23,24]. The manual spraying technique (*e.g.*, airbrush) is straightforward and cost-effective. However, it is relatively time-consuming and susceptible to operator variability, which may compromise the consistency of results. Sublimation can produce finely matrix crystal particles and uniform matrix deposition, but the absence of solvents in this method may hinder the effective detection of certain analytes within biological samples. Additionally, sublimation requires that the sublimation point of the matrix must be lower than its melting point, which also restricts its application. In contrast, automatic sprayer not only facilitates the formation of fine matrix crystals and uniform matrix coatings but also offers higher efficiency and superior reproducibility. Furthermore, it enables the deposition of matrices not suitable for sublimation. Consequently, automated spraying techniques integrate many advantages of both manual spraying and sublimation, positioning themselves as the most widely used matrix deposition techniques.

Currently, commonly used automatic matrix spraying devices encompass the ImagePrep [25–27] and HTX TM-Sprayer [11,28]. ImagePrep employs vibrational atomization technology to produce matrix aerosols [29], thereby promoting the uniform deposition of diminutive droplets onto the surfaces of tissue sections. Its average droplet size is approximately 20 μm, with all droplets measuring <50 μm [26,30]. In addition, it has been reported by Bruker that ImagePrep can achieve high-resolution imaging with a resolution of 50 μm [31]. Until now, ImagePrep is mainly applicable to MALDI imaging with a spatial resolution of 50 μm or lower [29,32,33]. Similarly, HTX TM-Sprayer represents another widely used automatic matrix spray instrument that incorporates thermal-controlled nozzle technology to produce fine mist [34]. This device utilizes pressurized heated nitrogen for the drying process to facilitate crystallization [35]. HTX TM-Sprayer also generates micron-scale crystalline particles [36,37]. To date, the HTX TM-Sprayer can be applied to higher resolution experiments (*ca.* 10 μm) [29,38]. Though the prevalent use of these spraying devices, the resultant crystals are predominantly within the micrometer range (from a few microns to tens of microns). As the laser beam size continues to decrease, the need for smaller matrix particle dimensions also increases to achieve higher resolution. A recent study has shown that transmission-mode MALDI-2 can achieve MSI of cells and tissues with subcellular resolution. Specifically, a pixel size of 600 nm was demonstrated in brain tissue [39]. Therefore, the advancement of a MALDI matrix spraying technique that is compatible with automated sprayers and capable of producing nanoscale crystal particles and uniform matrix coatings possesses substantial academic and practical significance.

To address this issue, we develop an innovative technique designated as cluster airflow assisted matrix coating (CAAMC). This technique integrates multiple cluster airflow channels within the same nozzle, thereby allowing converging airflows to concurrently interact with the matrix droplets. This design effectively disaggregates the droplets into smaller particles and promotes the formation of smaller matrix crystals. Since sublimation is currently the most effective method for producing fine matrix crystals and uniform matrix coatings, this experiment was conducted in comparison with the sublimation method. The results showed that CAAMC not only produces smaller nanoscale matrix crystals but also ensures a more uniform matrix deposition. It is worth noting that this signifies the first successful development of an automatic spraying technique for nano-matrix crystal particles. High-quality matrix coatings produced by CAAMC markedly enhance the imaging capabilities of compounds in rat brain tissue sections and single cells. Overall, CAAMC demonstrates significant potential for improving the sensitivity and spatial resolution of MALDI-MSI, suggesting important implications for the application of automatic spraying techniques in high-resolution imaging.

2,5-Dihydroxybenzoic (DHB), α-cyano-4-hydroxycinnamic acid (CHCA), 2-mercapto-benzothiazole (2-MBT), sinapic acid (SA), and 3,4-dimethoxycinnamic acid (DMCA) were procured from J&K Scientific Ltd. (Beijing, China). Other reagents were purchased from Sigma-Aldrich (St. Louis, MO) unless otherwise noted. A rat brain was procured from an 8-week-old male Sprague Dawley rat provided by the Shanghai Super-B&K Laboratory Animal Corp. Ltd. (Shanghai, China). U251 cells were provided by Beijing Tiantan Hospital, Capital Medical University. The utilization of animal tissues and cells adhered strictly to the protocols endorsed by the administrative guidelines of the Chinese Council on Animal Care, and all procedures were subject to the approval and oversight of the Ethics Committee of Minzu University of China (No. ECMUC2020004AA). More details about materials and reagents can be found in the Supporting information.

CAAMC was achieved by increasing the number of airflow channels. From a top-down perspective, the airflow channel is located in the periphery, while the passageway is positioned near the matrix outlet from a bottom-up perspective, indicating a directional convergence towards the nozzle tip. This technique was facilitated using a commercial matrix sprayer of HIT MatrixPrep (HIT Co., Ltd., Beijing, China) to incorporate a spray nozzle with multiple cluster airflow channels.

To attain the best deposition effect of CAAMC, the spray parameters were systematically refined by using an L9 (3^3) orthogonal array design. Detailed information is provided in Supporting information.

Four different matrices: DHB, 2-MBT, CHCA, and SA were deposited on the indium tin oxide (ITO)-coated glass slide using CAAMC and sublimation, respectively. Microscopic images of the crystal morphology were captured by a ZEISS GeminiSEM 300 (Carl Zeiss Jena, Oberkochen, Germany) at 10k× and 20k×. Detailed information about the preparation of the matrix solution is shown in the Supporting information.

To evaluate the quantitative accuracy of CAAMC as a matrix sprayer, an amino acid (phenylalanine, Phe) and a lipid (phosphatidylglycerol, (PG)(14:0/14:0)) were selected for linearity evaluation. Detailed steps can be found in Supporting information.

Fresh frozen rat brain tissue was cut into 12 μm slides in a Leica CM1860 cryostat (Leica Microsystems Inc., Wetzlar, Germany) and then freeze-thawed on ITO-coated conductive slides. It was then left to dry in a vacuum dryer for 30 min before the matrix was deposited.

U251 cells are a type of human glioma cells. The cell culture process is provided in Supporting information.

Before the application of the matrix, we weighed the clean blank slides to facilitate the calculation of the matrix coating weight. 2-MBT matrix solution was deposited onto the sample-mounted conductive glass slides by CAAMC and sublimation, respectively. CAAMC was installed on HIT MatrixPrep to spray matrix under the optimized conditions. Sublimation was performed in a sublimation apparatus (Chemglass Life Science, Vineland, NJ, USA). The detailed operation procedures of matrix sublimation are shown in Supporting information.

Tissue detection and imaging were carried out using the Autoflex Speed MALDI time-of-flight (TOF) mass spectrometer (Bruker Daltonics, Billerica, MA). For pinpointed imaging data acquisition of the targeted metabolites and lipids in rat brain tissue section, we employed a spatial resolution of 100 μm. For single-cell imaging, MSI was performed on the timsTOF fleX MALDI-2 in the positive

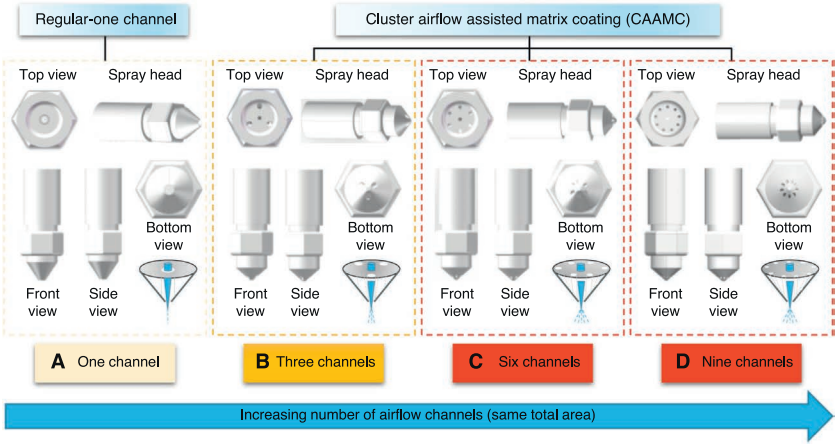


Fig. 1. Design of CAAMC. (A) Regular design with one airflow channel. (B) Three cluster airflow channels. (C) Six cluster airflow channels. (D) Nine cluster airflow channels.

ion mode using a 5×5 μm^2 pixel size. More detailed information can be found in Supporting information.

Bruker's FlexImaging software (version 4.1) facilitated the detailed reconstruction of ion maps for detectable endogenous molecules, allowing visualization of their spatial distribution within tissue sections. For single-cell imaging experiments on timsTOF fleX MALDI-2, MALDI-MSI data were imported into SCiLS Lab (version 2023b, Bruker Daltonics), and data visualization and analysis were conducted on TIC normalized data.

After MALDI-MSI, the tissue section was washed with different concentrations of EtOH. Histological staining and optical image capture were performed based on previously described procedures [40].

In alignment with previously established methodologies, we extracted total low-MW metabolites from rat brain (50 mg) and U251 cells (*ca.* 2×10^6 cells). The detailed extraction procedure and analytical method by LC-MS/MS are provided in Supporting information.

Statistical analysis was performed by one-way analysis of variance (ANOVA) using SPSS version 25 (IBM Corp., Armonk, USA). A value of $P < 0.05$ was considered to be significant ($^*P < 0.05$).

To obtain smaller crystal particles for improved MS resolution, we developed a novel matrix spraying technique named CAAMC. This technique increases the number of channels inside the nozzle tip, which allows single airflow to be divided into multiple airflows. As illustrated in Fig. 1, we present regular-one channel and three multiple channel configurations characterized by 3, 6, and 9 airflow channels. These airflow channels converge at the tip of the nozzle. Notably, the total cross-sectional area of the multiple airflow channels remains consistent with that of the regular-one channel. Based on the principles of the Continuity equation and Bernoulli's equation (Fig. S1 in Supporting information), it can be inferred that the negative pressure at the matrix nozzle in the CAAMC system increases, thereby promoting the atomization of the matrix droplets. This process facilitates the formation of finer matrix crystals. The detailed deduction process can be found in the section of "Design of CAAMC" (Supporting information). Additionally, the multiple airflows in the CAAMC induce impact and collision effects on the matrix droplets, further reducing their size and consequently resulting in the generation of smaller matrix crystals. Therefore, it is assumed that multiple cluster airflows can produce better matrix coatings than single airflow. To verify this hypothesis, a comparative experiment was conducted to assess the matrix crystals and uniformity of 2-MBT coated by CAAMC with 1, 3, 6, and 9 airflow channels, respectively. The results indicated that the use of multiple airflow channels could indeed yield superior matrix coatings compared to the traditional single-channel configuration (Fig. S2 in Supporting information). This may be due to that cluster airflow can collectively interact with the matrix solution, thereby fragmenting the matrix solution into smaller matrix droplets. These smaller droplets subsequently crystallize into finer crystal particles, resulting in a uniform matrix coating. To ensure the acquisition of high-fidelity data in subsequent experiments, it is imperative to further optimize the number of airflow channels as well as other relevant spraying parameters. To this end, an orthogonal array experiment was conducted to optimize the matrix spraying parameters. Three factors were selected for optimization: number of airflow channels, spray time, and gas pressure. Each factor was assigned three levels. The number of airflow channels was set to 3, 6, and 9; the spray time was designated as 4, 8, and 12 min; and the gas pressure was established at 0.3, 0.6, and 0.9 MPa. The results, as shown in Fig. S3 (Supporting information), identified the optimal conditions as having 6 airflow channels, a spray time of 8 min, and a gas pressure of 0.6 MPa. These parameters were utilized in the subsequent experiments.

Under optimized conditions, DHB, CHCA, 2-MBT, and SA were chosen for the comparison of CAAMC and a regular-one channel spraying technique. High-magnification scanning electron microscopy (SEM) allows for direct observation of the crystal sizes and uniformity of the matrix. As depicted in Fig. S4 (Supporting information), the four types of matrix particles produced by the regular-one channel spray were at the micron scale, substantially larger than the matrix particles generated by the CAAMC method. This finding confirms the superior capability of CAAMC in generating small particle sizes. To further demonstrate the advantages of CAAMC, we conducted a comparative analysis between CAAMC and sublimation. As illustrated in Fig. 2, the crystal particles produced by CAAMC are smaller than those generated by sublimation for the same matrix. Specially, DHB achieved an average size of only 76 ± 18 nm. CHCA particles fall within the nanoscale range of 120 ± 33 nm. Although sublimation also produces small nanoscale CHCA crystal particles (250 ± 57 nm), they are approximately twice the size of those produced by CAAMC. By contrast, 2-MBT crystals are larger than the above two matrices. CAAMC produced 2-MBT crystals averaging approximately 528 ± 125 nm, whereas the crystals obtained through sublimation mostly measure around 856 ± 224 nm. The 2-MBT crystalline particles produced by sublimation exhibit almost twice the crystal sizes of those produced by CAAMC. Moreover, SA matrix crystal particles produced by CAAMC (517 ± 130 nm) were also smaller than sublimation (992 ± 166 nm). Interestingly, the SA crystals produced by sublimation are also nearly twice the size as those produced by

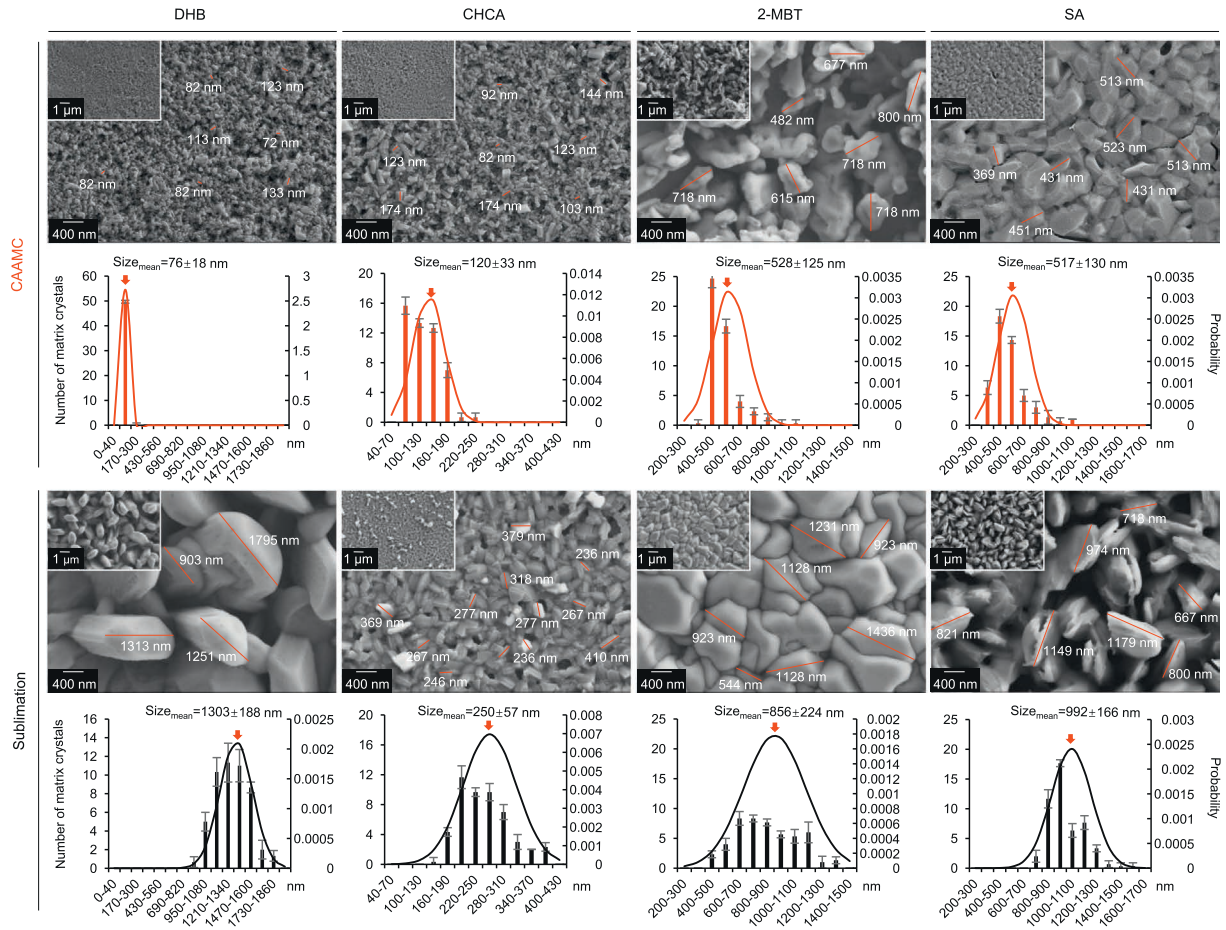


Fig. 2. SEM images of matrix crystal particle morphology. Crystal morphology of DHB, 2-MBT, CHCA, and SA sprayed by CAAMC and sublimation, respectively. The smaller images were captured at a magnification of 10k×, whereas the larger images were at a magnification of 20k× using SEM. Statistical analysis of crystal particles of DHB, 2-MBT, CHCA, and SA were shown under the corresponding SEM images. Statistical data were gathered using a five-point sampling method from the 10k× magnified images.

CAAMC. Overall, CAAMC demonstrates significant advantages over the widely used sublimation by effectively reducing the particle sizes of matrix crystals and enhancing the uniformity of matrix coating.

Quantitative accuracy studies represent another crucial aspect in evaluating the novel MALDI matrix coating method. This study selected Phe and PG(14:0/14:0) for quantitative analysis by MALDI-MS in the positive ion mode. Figs. S5 and S6 (Supporting information) illustrate the linear dynamic range, limit of detection (LOD), and limit of quantification (LOQ) for Phe and PG(14:0/14:0), respectively. In the range of 0.008-10 μg/mL, CAAMC demonstrated a good linear relationship between Phe concentration and detection intensity ($R^2 = 0.9995$) (Fig. S5A). At a signal-to-noise (S/N) threshold of 3, the LOD for Phe was determined to be 0.004 μg/mL (Fig. S5B). For sublimation, the concentration showed a linear relationship with detection intensity in the range of 0.006-10 μg/mL ($R^2 = 0.996$) (Fig. S5C), with an LOD of 0.004 μg/mL at an S/N ratio of 3 (Fig. S5D). For PG(14:0/14:0), CAAMC exhibited a good linear relationship between concentration and detection intensity in the range of 0.004–4 μg/mL ($R^2 = 0.9996$) (Fig. S6A). The LOD was found to be 0.002 μg/mL when the S/N ratio threshold was set at 3 (Fig. S6B). In contrast, the concentration and detection intensity for sublimation displayed a linear relationship over the range of 0.004–2 μg/mL ($R^2 = 0.995$) (Fig. S6C), with an LOD for PG(14:0/14:0) at 0.002 μg/mL under the same condition (Fig. S6D). Overall, CAAMC as a matrix coating technique exhibited outstanding quantitative performance for both the Phe and PG(14:0/14:0). The results demonstrated a strong linear correlation between concentration and detection intensity with a low concentration limit of 0.002 μg/mL and a high concentration limit of 10 μg/mL. This indicates that CAAMC has significant potential for *in situ* quantification of endogenous compounds in biological samples by MALDI-MS.

To better clarify the good performance of CAAMC, a systematic quantitative analysis of the lipid PE(17:0) was conducted in the hippocampus region of rat brain tissues, a key area of the rat brain, to compare the three matrix deposition methods. The results, as illustrated in Fig. S7 (Supporting information), demonstrated that CAAMC significantly outperformed regular-one channel and sublimation in terms of quantitative accuracy. Furthermore, to validate the superiority of CAAMC, we employed microarray technique [41] to analyze PE(17:0) in homogenized rat brain tissue samples. The findings also revealed that the good detection performance of CAAMC in the homogenized tissue. These experimental results provide compelling evidence for the advantages of CAAMC in quantitative analysis, highlighting its significant improvements in both accuracy and reliability of lipid detection in the brain micro-region and tissues.

Furthermore, the assessment of CAAMC's reproducibility and robustness also serves as a vital criterion for evaluating its overall reliability and efficacy. Microarray technique was again used to prepare rat liver tissues [41]. Then these parallel tissue microarrays were separately subjected to 2-MBT matrix spraying by CAAMC at five distinct time points (07:00, 10:00, 13:00, 16:00, and 19:00),

followed by detection using MALDI-MS (Fig. S8 in Supporting information). Each experimental condition was performed in triplicate ($n = 3$). The results demonstrated that the number of detected compounds at each time point was comparable, with no significant differences observed. Furthermore, fifteen representative compounds were selected for intensity analysis, and one-way ANOVA was conducted. The statistical analysis revealed that all compounds exhibited *P*-values greater than 0.05, indicating no statistically significant differences in compound intensities across different spraying times (Table S1 in Supporting information). These findings confirm that the CAAMC technique exhibits high reproducibility and good robustness.

To investigate the efficiency of CAAMC on the imaging of compounds within tissues, this study deposited 2-MBT onto rat brain tissue slices adhered to ITO-coated conductive glass slides employed CAAMC and sublimation, respectively. In order to make a fair comparison between the two methods, the mass per unit area of the matrix coatings was kept almost consistent and both controlled in the optimal amount, as shown in Fig. S9 (Supporting information). The amount of matrix applied was controlled within the range of 0.1–0.2 mg/cm^2, corresponding to the optimal coating amount reported for imaging [42]. Under the experimental conditions, MALDI analysis was performed on rat brain tissue and single-cell samples prepared using three different spraying methods. As shown in Fig. S10 (Supporting information), CAAMC significantly outperformed regular-one channel and sublimation in terms of the number of detectable signals and total signal intensity. These findings demonstrate the potential of CAAMC to enhance MALDI ionization efficiency and detection sensitivity, highlighting its important application prospects in MALDI-MS analysis of biological samples. Subsequently, the left hemisphere of the rat brain tissue section by sublimation and the right hemisphere of the adjacent rat brain tissue section by CAAMC were subjected to MALDI analysis and imaging. As shown in Fig. S11 (Supporting information), the CAAMC method demonstrates superior performance compared to sublimation techniques in terms of signal intensity and the clarity of regional heterogeneity in compound imaging, exhibiting more pronounced advantages. The detailed results are show in the section of "MALDI-MSI of compounds in rat brain at the lateral resolution of 100 μm by CAAMC and sublimation" (Supporting information). To further validate the superiority of the CAAMC technique, we conducted a 5 μm lateral resolution imaging experiment of compounds in rat brain tissue. Furthermore, we added a comparative analysis with regular-one channel to more effectively highlight the advantages of the CAAMC. As shown in Fig. 3, hematoxylin-eosin (HE)-stained images identify three regions of interest, delineated by white boxes, primarily encompassing the cerebellar gray and white matter. The imaging results reveal that compounds [glycerophosphocholine+K]$^+$ at *m/z* 296.0660, [cer(d42:0)+Na]$^+$ at *m/z* 652.6017, and [PC(38:1)+K]$^+$ at *m/z* 854.6029 predominantly localize within gray matter, whereas compounds [lysoPA(18:1)+Na]$^+$ at *m/z* 459.2488, [lysoPC(16:0)+H]$^+$ at *m/z* 496.3430, and [PC(32:0)+H]$^+$ at *m/z* 734.5713 are mainly distributed in white matter. Specifically, the images obtained *via* CAAMC demonstrate markedly higher signal quality compared to those acquired by regular-one channel spraying and sublimation methods. For instance, under CAAMC, [glycerophosphocholine+K]$^+$ exhibits the highest distribution intensity within gray matter, with clear delineation at the gray-white matter boundary and no evident signal delocalization. In contrast, images from the regular-one channel method exhibit weaker signals, blurred boundaries, and noticeable delocalization phenomena. Although sublimation avoids delocalization, the signal intensity of [glycerophosphocholine+K]$^+$ within gray matter is insufficient, resulting in lower image quality. Similarly, for [cer(d42:0)+Na]$^+$, CAAMC provides robust signals in gray matter with a clean background in white matter, whereas

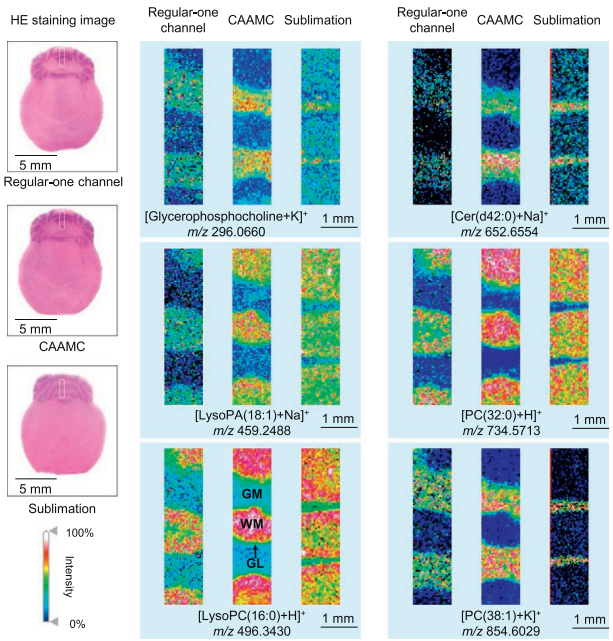


Fig. 3. Comparison of regular-one channel, CAAMC, and sublimation on the MALDI-MSI of small molecules and lipids in rat brain tissue sections. Reconstructed ion images of selected compounds detected in rat brain tissue sections. MS imaging was acquired at 5 μm spatial resolution. Scale bar: 1 mm.

the regular-one channel approach produces a clear background in white matter but significantly lower signals in gray matter accompanied by delocalization. Although sublimation yields signals of comparable intensity with CAAMC in gray matter, the boundary between white and gray matter remains indistinct, compromising image clarity. For [PC(38:1)+K]$^+$, all spraying methods demonstrated relatively distinct regional boundaries, with CAAMC producing the highest signal intensity and the clearest images. In comparison, the regular-one channel approach exhibits some delocalization, while sublimation produces ion signals slightly weaker than CAAMC. Regarding [lysoPA(18:1)+Na]$^+$, [lysoPC(16:0)+H]$^+$, and [PC(32:0)+H]$^+$ which are localized within white matter, images obtained by CAAMC show higher signal intensities than the other two methods. Notably, [lysoPC(16:0)+H]$^+$ and [PC(32:0)+H]$^+$ display clearly discernible distribution within the granular layer (GL), located at the periphery of white matter. This fine structural detail is difficult to distinguish using regular-one channel or sublimation techniques, highlighting the high spatial resolution and structural fidelity afforded by CAAMC. This phenomenon can be attributed to the reduced matrix crystal particle size achieved by CAAMC. The nanoscale matrix crystals facilitate more homogeneous co-crystallization with analytes, thereby enhancing ionization efficiency of analytes through sufficient energy transfer. Compared to sublimation, CAAMC employs solvent-mediated matrix dissolution, enabling enhanced analyte solubilization and subsequent co-crystallization. In contrast, the solvent-free environment of sublimation-based matrix deposition imposes fundamental limitations on compound dissolution efficiency, potentially leading to undetected analytes in mass spectrometric analysis. In addition, the sublimation process exhibits an exceptionally short crystallization time, which may consequently compromise crystal formation efficiency. In summary, CAAMC surpasses regular-one channel and sublimation methods in both signal intensity and spatial resolution, enabling detailed visualization of compound distribution across different brain regions. These results underscore its potential and advantages for high-resolution MALDI imaging. The detailed information about the ion signals is available in Tables S2 and S3 (Supporting information).

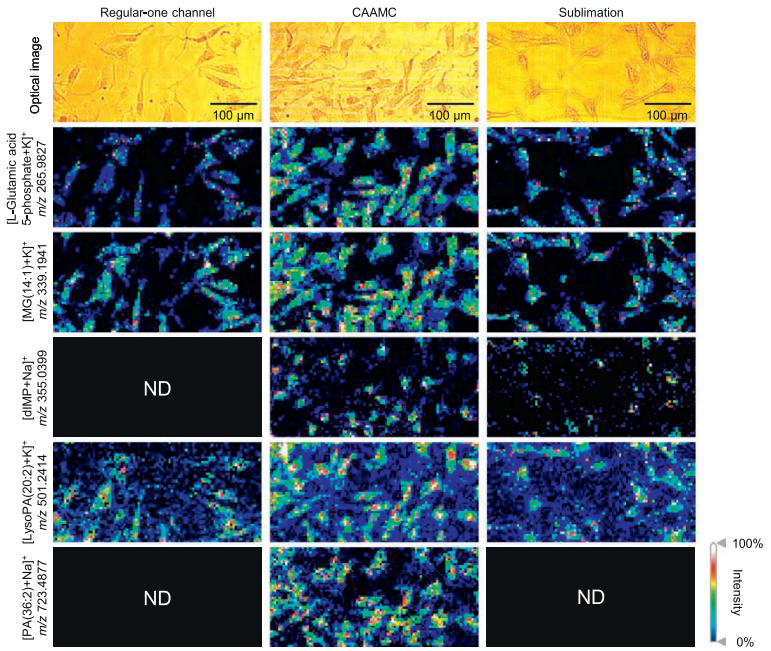


Fig. 4. Comparison of regular-one channel, CAAMC, and sublimation on the MALDI-MSI of small molecules and lipids in single cells. Reconstructed ion images of selected compounds detected in U251 cells. MS imaging was acquired at 5 μm spatial resolution. Scale bar: 100 μm.

To further verify the advantages of CAAMC, single-cell imaging was evaluated. We deposited 2-MBT onto ITO-coated conductive glass slides containing single cells using regular-one channel, CAAMC, and sublimation, respectively. Similarly, the matrix mass per unit area was maintained within the optimal range for imaging quality (Fig. S9). Then these three coated samples were subjected to MALDI analysis and imaging. The experimental results were depicted in Fig. 4. Five representative compounds were presented, accompanied by corresponding optical images to facilitate comparison of the imaging performance across different matrix coating techniques. The images obtained using the CAAMC method indicate that [L-glutamic acid 5-phosphate+K]$^+$ at *m/z* 265.9827, [MG(14:1)+K]$^+$ at *m/z* 339.1941, [lysoPA(20:2)+K]$^+$ at *m/z* 501.2414, and [PA(36:2)+Na]$^+$ at *m/z* 723.4877 predominantly distribute throughout the entire cellular region. In contrast, [dIMP+Na]$^+$ at *m/z* 355.0399 primarily localizes within the cell nucleus. This suggests that the CAAMC enables a comprehensive capture of the spatial distribution of compounds within cells, with particularly high fidelity for nuclear localization. Specifically, [L-glutamic acid 5-phosphate+K]$^+$, [MG(14:1)+K]$^+$, and [lysoPA(20:2)+K]$^+$ imaged *via* CAAMC exhibited clear cellular structures, with high overall signal intensity and distinct differences between the nuclear and cytoplasm. The imaging results closely correspond to the optical images, demonstrating high reliability. Conversely, results from regular-one channel and sublimation methods showed generally weaker signals, especially within the nucleus, which compromised the integrity of cell morphology and resulted in inferior image quality compared to CAAMC. Furthermore, this was even more evident for [dIMP+Na]$^+$, where the sublimation method detected only sparse and weak signals, while regular-one channel imaging failed to resolve its distribution entirely. In addition, for [PA(36:2)+Na]$^+$, both the regular-one channel and sublimation techniques failed to produce effective imaging results, preventing accurate assessment of its intracellular distribution. These findings robustly demonstrate the superiority of the CAAMC technique for high-resolution imaging of compounds within cells. More information about the ion signals is available in Tables S4 and S5 (Supporting information).

In addition, we conducted a comparison of CAAMC with two commonly used and popular automatic spraying techniques, HTX TM-Sprayer and ImagePrep, in terms of sensitivity and spatial resolution. As shown in Fig. S12 (Supporting information), CAAMC outperforms the popular methods HTX TM-Sprayer and ImagePrep in the sensitivity (limit of detection) and high-resolution imaging (5 μm). In summary, CAAMC represents a significant technical advancement in automatic spray techniques. The successful application of this automatic matrix spray technique in single-cell imaging offers considerable potential for exploring smaller units of life, such as smaller cells and subcellular structures. This capability could lead to new insights into cellular processes, interactions, and functions, ultimately advancing our understanding of complex biological systems and paving the way for innovations in medicine and biotechnology.

In conclusion, CAAMC can produce smaller matrix crystals and uniform matrix coatings compared to those generated by regular-one channel and sublimation, representing a significant advancement in the application of automatic spray devices. Specifically, the particle sizes of the DHB, CHCA, 2-MBT, and SA matrix crystals produced by CAAMC were measured to be <100, 150, 650, 650 nm, respectively, whereas regular-one channel and sublimation mainly produces matrix crystal sizes of micron-sized particles. It is evident that for the same matrix, the matrix crystals obtained through CAAMC are consistently smaller than those obtained *via* regular-one channel and sublimation. This advantage significantly enhanced the sensitivity and resolution of MALDI-MSI, which is of great importance for spatial omics research. In summary, the development of CAAMC marks a successful application of automatic spraying technology in high-resolution MALDI-MSI, which is expected to become a standard practice in spatial omics studies of small biological units.

Declaration of competing interest

The authors declare that they have no known competing financial interests or personal relationships that could have appeared to influence the work reported in this paper.

CRediT authorship contribution statement

Hua Guo: Writing – review & editing, Writing – original draft, Visualization, Validation, Supervision, Software, Resources, Project administration, Methodology, Investigation. **Ran Wu:** Writing – review & editing, Supervision, Methodology. **Qichen Hao:** Software, Methodology. **Liang Qin:** Supervision, Project administration, Methodology. **Lulu Chen:** Writing – review & editing, Writing – original draft. **Hao Hu:** Writing – review & editing, Writing – original draft, Software, Methodology, Investigation. **Jie Feng:** Writing – review & editing, Methodology. **Lei Wang:** Software, Methodology. **Rui Liu:** Writing – review & editing, Writing – original draft, Methodology. **Difan Chen:** Supervision. **Anna Wang:** Writing – review & editing, Writing – original draft. **Zihan Wang:** Writing – review & editing, Writing – original draft. **Xiangrui Cheng:** Writing – review & editing, Writing – original draft. **Shuyu Hao:** Writing – review & editing, Writing – original draft, Methodology. **Xiaodong Wang:** Writing – review & editing, Writing – original draft, Supervision, Project administration, Methodology, Investigation, Funding acquisition, Conceptualization. **Huaqing Zhang:** Writing – review & editing, Funding acquisition. **Gaopeng Li:** Writing – review & editing, Project administration.

Acknowledgments

This work was supported by the Key Research and Development Program of Zhejiang Province (No. 2025C01135), the National Natural Science Foundation of China (Nos. 31770384 and 21605164), the Youth Academic Team Project of MUC (No. 1030102200301), the Huayi Technology Innovation Center for Research Resources (No. HTIC P01RR2017001A), and the Key Laboratory Construction Funds of State Ethnic Affairs Commission of China (No. 10301–02200303).

Supplementary materials

Supplementary material associated with this article can be found, in the online version, at doi:10.1016/j.cclet.2025.112335.

References

[1] X.Y. Guo, W.B. Cao, X.M. Fan, et al., Angew. Chem. Int. Ed. 62 (2023) e202214804.
[2] M. Schwaiger-Haber, E. Stancliffe, D.S. Anbukumar, et al., Nat. Commun. 14 (2023) 2876.
[3] L.L. Chen, Y. Zhang, Q.C. Hao, et al., New Phytol. 243 (2024) 2021–2036.
[4] Z. Sun, F.F. Wang, Y.W. Liu, et al., TrAC Trend. Anal. Chem. 175 (2024) 117727.
[5] Y. Liu, G. Li, T.J. Gu, L. Li, Anal. Chem. 94 (2022) 3774–3781.
[6] R. Wu, D.X. Jiang, H. Hu, et al., Chin. Chem. Lett. 35 (2024) 109624.
[7] H. Xu, M. Han, H. Liu, et al., Chin. Chem. Lett. 35 (2024) 109095.
[8] M. Vandenbosch, S.M. Mutuku, M.J.Q. Mantas, et al., Anal. Chem. 95 (2023) 18719–18730.
[9] G. Li, Q. Cao, Y. Liu, et al., Rapid Commun. Mass Sp. 33 (2019) 327–335.
[10] P. Xie, J. Chen, Y. Xia, Z. Cai, Chin. Chem. Lett. 36 (2025) 110595.
[11] G. Guo, M. Papanicolaou, N.J. Demarais, et al., Nat. Commun. 12 (2021) 3241.
[12] G. Li, F. Ma, Q. Cao, et al., Nat. Commun. 10 (2019) 4697.
[13] Z. Lingpeng, H. Yanyi, W. Guanbo, Chin. Chem. Lett. 35 (2024) 108685.
[14] R.N. Alolga, S.L. Wang, L.W. Qi, et al., TrAC Trend. Anal. Chem. 178 (2024) 117860.
[15] C. Villette, L. Maurer, J. Zumsteg, et al., Nat. Commun. 14 (2023) 4244.
[16] W. Zhang, Z. Xu, G. Dai, et al., Chin. Chem. Lett. 35 (2024) 109135.
[17] Q. He, C.R. Sun, J. Liu, Y.J. Pan, TrAC Trend, Anal. Chem. 136 (2021) 116183.
[18] X. Han, Y. Yang, J. Lu, et al., Chin. Chem. Lett. 36 (2025) 110183.
[19] C. Jing, X. Peisi, W. Pengfei, et al., Chin. Chem. Lett. 35 (2024) 108895.
[20] X.L. Pei, X.N. Liu, J.L. Du, et al., Int. J. Mass Spectrom. 455 (2020) 116373.
[21] P. Bourceau, B. Geier, V. Suerdieck, et al., Nat. Protoc. 18 (2023) 3050–3079.
[22] D.C. Castro, Y.R. Xie, S.S. Rubakhin, et al., Nat. Methods 18 (2021) 1233–1238.
[23] S. Heuckeroth, A. Behrens, C. Wolf, et al., Nat. Commun. 14 (2023) 7495.
[24] E. Yang, X.E. Shen, H. West-Foyle, et al., Adv. Sci. 10 (2023) 2304343.
[25] Q.Q. Shi, H. Yin, R.D. Song, et al., Nat. Chem. 15 (2023) 257–270.
[26] P.S. Xie, C. Zhao, X.P. Liang, et al., Anal. Chem. 92 (2020) 7413–7418.
[27] M. Duhamel, L. Drelich, M. Wisztorski, et al., Nat. Commun. 13 (2022) 6665.
[28] R. Shariatgorji, A. Nilsson, E. Fridjonsdottir, et al., Nat. Protoc. 16 (2021) 3298–3321.
[29] C. Zhao, Z. Cai, Mass Spectrom. Rev. 41 (2022) 469–487.
[30] Š. Strnad, V. Pražienková, D. Sýkora, et al., Talanta 201 (2019) 364–372.
[31] M. Schuerenberg, C. Luebbert, S.O. Deininger, et al., Nat. Methods 4 (2007) 462-462.
[32] C. Houdelet, K. Arafah, M. Bocquet, P. Bulet, Proteomics 22 (2022) e2100224.
[33] K.N.S. Laura, J. Castellanos-Garcia, Jeerapat Doungchawee, Richard W. Vachet, Analyst 146 (2021) 7720–7729.
[34] L.W. Meng, J. Han, J.Y. Chen, et al., Anal. Chem. 94 (2022) 6457 -6462.
[35] Q.C. Zang, M.J.C. Wang, Y. Zhu, et al., Anal. Chem. 93 (2021) 15373–15380.
[36] L.H. Tucker, A. Conde-González, D. Cobice, et al., Anal. Chem. 90 (2018) 8742–8749.
[37] L. Meng, J. Han, J. Chen, et al., Anal. Chem. 94 (2022) 6457 -6462.
[38] C. Cumin, L. Gee, T. Litfin, et al., Anal. Chem. 96 (2024) 11163–11171.
[39] M. Niehaus, J. Soltwisch, M.E. Belov, K. Dreisewerd, Nat. Methods 16 (2019) 925–931.
[40] R. Casadonte, R.M. Caprioli, Nat. Protoc. 6 (2011) 1695–1709.
[41] H. Huang, H. Liu, W. Ma, et al., Plant Biotechnol. J. 21 (2023) 2574–2584.
[42] R. Fernandez, J. Garate, L. Martin-Saiz, et al., Anal. Chem. 91 (2019) 803–807.